J|A|C|S
ARTICLES
Published on Web 05/08/2007

Substrate- and Isoform-Specific Dioxygen Complexes of Nitric Oxide Synthase

David Li,[†] Mariam Kabir,[†] Dennis J. Stuehr,[‡] Denis L. Rousseau,*[,†] and Syun-Ru Yeh*[,†]

Contribution from the Department of Physiology and Biophysics, Albert Einstein College of Medicine of Yeshiva University, Bronx, New York 10461, and Department of Immunology, Lerner Research Institute, Cleveland Clinic, Cleveland, Ohio 44195

Received January 30, 2007; E-mail: rousseau@aecom.yu.edu; syeh@aecom.yu.edu

Abstract: Nitric oxide synthase (NOS) catalyzes the formation of NO via a consecutive two-step reaction. In the first step, L-arginine (Arg) is converted to *N*-hydroxy-L-arginine (NOHA). In the second step, NOHA is further converted to citrulline and nitric oxide (NO). To assess the mechanistic differences between the two steps of the reaction, we have used resonance Raman spectroscopy combined with a homemade continuous-flow rapid solution mixer to study the structural properties of the metastable dioxygen-bound complexes of the oxygenase domain of inducible NOS ($iNOS_{oxy}$). We identified the O−O stretching frequency of the substrate-free enzyme at 1133 cm^{-1}. This frequency is insensitive to the presence of tetrahydrobiopterin, but it shifts to 1126 cm^{-1} upon binding of Arg, which we attribute to H-bonding interactions to the terminal oxygen atom of the heme iron-bound dioxygen. In contrast, the addition of NOHA to the enzyme did not bring about a shift in the frequency of the O−O stretching mode, because, unlike Arg, there is no H-bond associated with the terminal oxygen atom of the dioxygen. The substrate-specific H-bonding interactions play a critical role in determining the fate of the key peroxy intermediate. In the first step of the reaction, the H-bonds facilitate the rupture of the O−O bond, leading to the formation of the active ferryl species, which is essential for the oxidation of the Arg. On the other hand, in the second step of the reaction, the absence of the H-bonds prevents the premature O−O bond cleavage, such that the peroxy intermediate can perform a nucleophilic addition reaction to the substrate, NOHA.

Introduction

Nitric oxide synthase (NOS) catalyzes the formation of nitric oxide (NO) from oxygen and L-arginine (Arg) via a sequential two-step reaction by using NADPH as the electron source.[1−5] In the first step of the reaction, Arg is hydroxylated to *N*-hydroxy-arginine (NOHA), and in the second step, NOHA is oxidized to citrulline and NO. The three major isoforms, iNOS, eNOS, and nNOS (inducible, endothelial, and neuronal nitric oxide synthase, respectively), found in macrophages, endothelial cells, and neuronal tissues, produce NO that functions as a cytotoxic agent, a vasodilator, and a neurotransmitter, respectively.[6,7] The homodimeric enzyme consists of a reductase domain that binds FMN, FAD, and NADPH and an oxygenase domain that binds the heme and tetrahydrobiopterin (H4B) cofactors. During catalysis, mediated by calcium/calmodulin, electrons flow from NADPH through FAD and FMN in the reductase domain of one subunit of the homodimer to the oxygenase domain of the other subunit.[8,9] The crystal structures of the oxygenase domains of all three isoforms have been determined.[10−13] They show that the heme is coordinated by a cysteine residue on the proximal side, as in cytochrome P450-type enzymes, and the substrates, Arg or NOHA, bind above the heme iron atom in the distal pocket, while the cofactor, H4B, binds along the side of the heme.

In the H4B-bound resting state of NOS, the heme is primarily five-coordinate (5C) with a minor six-coordinate (6C) component. Substrate (Arg or NOHA) binding fully converts the enzyme to the 5C configuration similar to that observed in the cytochrome P450s.[14−17] A generally accepted reaction scheme for NOS is illustrated in Figure 1. In this mechanism, the ferric H4B-bound heme (I) is first reduced to the ferrous form (II) by

[†] Albert Einstein College of Medicine of Yeshiva University.
[‡] Cleveland Clinic.

(1) Stuehr, D. J. *Biochim. Biophys. Acta* **1999**, *1411*, 217−230.
(2) Masters, B. S.; McMillan, K.; Sheta, E. A.; Nishimura, J. S.; Roman, L. J.; Martasek, P. *FASEB J.* **1996**, *10*, 552−558.
(3) Alderton, W. K.; Cooper, C. E.; Knowles, R. G. *Biochem. J.* **2001**, *357*, 593−615.
(4) Marletta, M. A. *Adv. Exp. Med. Biol.* **1993**, *338*, 281−284.
(5) Xie, Q. W.; Cho, H.; Kashiwabara, Y.; Baum, M.; Weidner, J. R.; Elliston, K.; Mumford, R.; Nathan, C. *J. Biol. Chem.* **1994**, *269*, 28500−28505.
(6) Nathan, C.; Xie, Q. W. *Cell* **1994**, *78*, 915−918.
(7) Billiar, T. R. *Ann. Surg.* **1995**, *221*, 339−349.
(8) Siddhanta, U.; Presta, A.; Fan, B.; Wolan, D.; Rousseau, D. L.; Stuehr, D. J. *J. Biol. Chem.* **1998**, *273*, 18950−18958.
(9) Panda, K.; Ghosh, S.; Stuehr, D. J. *J. Biol. Chem.* **2001**, *276*, 23349−23356.
(10) Crane, B. R.; Arvai, A. S.; Ghosh, D. K.; Wu, C.; Getzoff, E. D.; Stuehr, D. J.; Tainer, J. A. *Science* **1998**, *279*, 2121−2126.
(11) Raman, C. S.; Li, H.; Martasek, P.; Kral, V.; Masters, B. S.; Poulos, T. L. *Cell* **1998**, *95*, 939−950.
(12) Li, H.; Raman, C. S.; Glaser, C. B.; Blasko, E.; Young, T. A.; Parkinson, J. F.; Whitlow, M.; Poulos, T. L. *J. Biol. Chem.* **1999**, *274*, 21276−21284.
(13) Fischmann, T. O.; Hruza, A.; Niu, X. D.; Fossetta, J. D.; Lunn, C. A.; Dolphin, E.; Prongay, A. J.; Reichert, P.; Lundell, D. J.; Narula, S. K.; Weber, P. C. *Nat. Struct. Biol.* **1999**, *6*, 233−242.

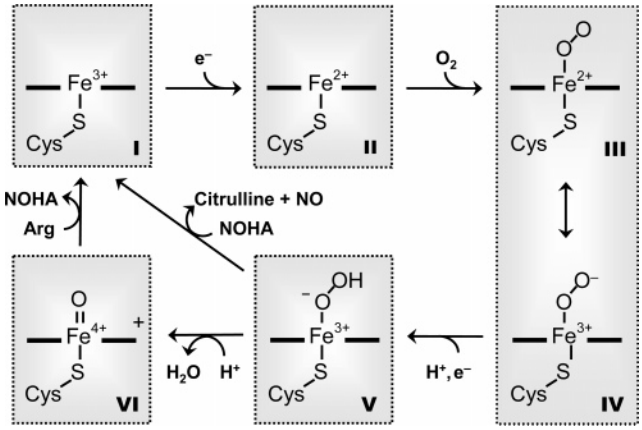

Figure 1. Schematic illustration of the NOS reaction mechanism. For details see the text.

accepting one electron from NADPH. It is followed by the binding of an oxygen molecule to the heme iron to form the oxy complex (III). The electron density on the heme iron in the oxy complex is redistributed to the dioxygen, leading to a ferric superoxide species (IV). The ferric superoxide species is subsequently reduced to a hydroperoxy species (V) by accepting an electron (possibly also a proton) from the H4B cofactor,[18] which is eventually rereduced by the reductase domain.[19] The efficient reduction of the superoxide by H4B, instead of by a direct electron transfer from the reductase domain, is believed to decrease the possibility of releasing the toxic superoxide into the cellular environment, as well as to increase the coupling efficiency of the oxygen chemistry and NO synthesis. The subsequent heterolytic cleavage of the O−O bond in the hydroperoxy species leads to a ferryl species with a π-cation radical on the porphyrin ring (VI). The ferryl species is the active oxygen intermediate that hydroxylates the Arg, via a P450-like oxygen insertion reaction. At the end of this reaction, NOHA is produced and the heme iron is converted back to the ferric form (I).

The second step of the reaction was initially believed to proceed via a different mechanism, owing to the requirement of only a single electron, which is insufficient for the formation of a ferryl species.[20,21] However, it was recently demonstrated that, like the first step of the reaction, the H4B transiently donates an electron, reducing the oxy species to a peroxy intermediate.[22] The peroxy species then either converts to a compound I type of intermediate, like the first step of the reaction, or it attacks NOHA via a nucleophilic addition reaction, either of which leads to the production of citrulline and NO.

There is now a general consensus that the sequential conversion from species I to V is essentially the same for both steps of the NOS reaction (Figure 1). Since the decay of the primary oxy complex (species IV) is slower than the decays of the subsequent intermediates,[23] none of the latter intermediates have been detected during the turnover of the reaction. Hence, it remains unclear whether or not the remaining steps of the reactions follow similar mechanisms. Nonetheless, with an elegant cryoreduction method, Davydov et al. recently identified a peroxy intermediate in the presence of either Arg or NOHA with EPR and ENDOR spectroscopies, although the protonated counterpart was not observed.[24]

In contrast to the other oxygen intermediates, the primary oxy complexes of the various NOS isoforms have been widely studied with optical absorption spectroscopy, by stabilizing it at low temperature or by capturing it in real-time with time-resolved measurements.[23,25−29] Although informative, conflicting data were reported (see the review in ref 30 and references therein). By simultaneously probing the oxy derivatives with optical absorption and resonance Raman spectroscopy, a more recent study of the oxygenase domain of nNOS ($nNOS_{oxy}$) revealed a Soret maximum at 430 nm and an O−O stretching mode (ν_{O-O}) at ∼1135 cm^{-1}, demonstrating the ferric−superoxide character of the oxy complex.[30,31] In this work, with similar techniques, we examined the oxy complexes of the oxygenase domain of iNOS ($iNOS_{oxy}$) to investigate if the binding of substrates and cofactor perturb its chemical and structural properties and if there are any isoform-specific characteristics of the iron−superoxide complex with respect to $nNOS_{oxy}$. To gain additional insight about the ligand−protein interactions in the two NOS isoforms under the various substrates and cofactor-bound states, resonance Raman studies of the CO derivatives were carried out as comparisons. The data revealed subtle differences in the electrostatic environments of the heme-bound ligand in the two NOS isoforms and their differential responses to substrate binding.

Materials and Methods

EPPS, Arg, NOHA, and sodium dithionite were purchased from Sigma (St. Louis, MO). H4B was purchased from Schircks Laboratories (Jona, Switzerland). The natural abundant gases, Ar, CO, and O_2, were obtained from Tech Air (White Plains, NY). The isotopically labeled $^{18}O_2$ was supplied by Icon (Mount Marion, NY).

The oxygenase domain of inducible nitric oxide synthase ($iNOS_{oxy}$) was expressed in *Escherichia coli* and purified in the absence of both Arg and H4B as described previously.[32] The enzyme was kept in EPPS buffer containing 10% glycerol at pH 7.6 and stored under liquid nitrogen until use. Prior to use, the protein was washed three times with 40 mM EPPS buffer at pH 7.6 using a centrifugal filtration unit

(14) Wang, J.; Stuehr, D. J.; Ikeda-Saito, M.; Rousseau, D. L. *J. Biol. Chem.* **1993**, *268*, 22255−22258.
(15) Wu, C.; Zhang, J.; Abu-Soud, H.; Ghosh, D. K.; Stuehr, D. J. *Biochem. Biophys. Res. Commun.* **1996**, *222*, 439−444.
(16) Martasek, P.; Liu, Q.; Liu, J.; Roman, L. J.; Gross, S. S.; Sessa, W. C.; Masters, B. S. *Biochem. Biophys. Res. Commun.* **1996**, *219*, 359−365.
(17) Roman, L. J.; Sheta, E. A.; Martasek, P.; Gross, S. S.; Liu, Q.; Masters, B. S. *Proc. Natl. Acad. Sci. U.S.A.* **1995**, *92*, 8428−8432.
(18) Hurshman, A. R.; Marletta, M. A. *Biochemistry* **2002**, *41*, 3439−3456.
(19) Hurshman, A. R.; Krebs, C.; Edmondson, D. E.; Huynh, B. H.; Marletta, M. A. *Biochemistry* **1999**, *38*, 15689−15696.
(20) Marletta, M. A. *J. Biol. Chem.* **1993**, *268*, 12231−12234.
(21) Pufahl, R. A.; Wishnok, J. S.; Marletta, M. A. *Biochemistry* **1995**, *34*, 1930−1941.
(22) Wei, C. C.; Wang, Z. Q.; Hemann, C.; Hille, R.; Stuehr, D. J. *J. Biol. Chem.* **2003**, *278*, 46668−46673.
(23) Abu-Soud, H. M.; Gachhui, R.; Raushel, F. M.; Stuehr, D. J. *J. Biol. Chem.* **1997**, *272*, 17349−17353.
(24) Davydov, R.; Ledbetter-Rogers, A.; Martasek, P.; Larukhin, M.; Sono, M.; Dawson, J. H.; Masters, B. S.; Hoffman, B. M. *Biochemistry* **2002**, *41*, 10375−10381.
(25) Bec, N.; Gorren, A. C.; Voelker, C.; Mayer, B.; Lange, R. *J. Biol. Chem.* **1998**, *273*, 13502−13508.
(26) Sato, H.; Sagami, I.; Daff, S.; Shimizu, T. *Biochem. Biophys. Res. Commun.* **1998**, *253*, 845−849.
(27) Ledbetter, A. P.; McMillan, K.; Roman, L. J.; Masters, B. S.; Dawson, J. H.; Sono, M. *Biochemistry* **1999**, *38*, 8014−8021.
(28) Gorren, A. C.; Bec, N.; Schrammel, A.; Werner, E. R.; Lange, R.; Mayer, B. *Biochemistry* **2000**, *39*, 11763−11770.
(29) Sorlie, M.; Gorren, A. C.; Marchal, S.; Shimizu, T.; Lange, R.; Andersson, K. K.; Mayer, B. *J. Biol. Chem.* **2003**, *278*, 48602−48610.
(30) Rousseau, D. L.; Li, D.; Couture, M.; Yeh, S. R. *J. Inorg. Biochem.* **2005**, *99*, 306−323.
(31) Couture, M.; Stuehr, D. J.; Rousseau, D. L. *J. Biol. Chem.* **2000**, *275*, 3201−3205.
(32) Ghosh, D. K.; Wu, C.; Pitters, E.; Moloney, M.; Werner, E. R.; Mayer, B.; Stuehr, D. J. *Biochemistry* **1997**, *36*, 10609−10619.

(Ultrafree-15, Biomax-10K NMWL membrane from Millipore) to remove glycerol. The final protein concentrations were determined by measuring the absorbance at 397 nm of the ferric enzyme in the presence of Arg and H4B using an extinction coefficient of 71 mM^{-1} cm^{-1}.[33] When necessary, H4B, Arg, and NOHA were added in 25-, 200-, and 25-fold excess, respectively, over the concentration of the protein and incubated overnight (~12 h) at room temperature. The difference in the concentrations of the substrates was used to reflect the factor of 4 higher affinity of the enzyme for NOHA as compared to L-Arg (K_d ~1.5 vs 5.8 μM, respectively).[18] The binding of Arg, NOHA, and H4B was confirmed by monitoring changes in the spin and coordination state of the ferric protein with optical absorption spectroscopy. The protein concentration for each sample was ~80 and 40−60 μM for the equilibrium and kinetic measurements, respectively. For equilibrium resonance Raman spectroscopic measurements of the CO derivatives, the samples were first purged with N_2 gas in an anaerobic cell. To form the ferrous−CO complexes, the purged samples were reduced with sodium dithionite, followed by injection of 400 μL of 1 atm CO by using a Hamilton (Reno, NV) gastight syringe.

The oxy intermediates of $iNOS_{oxy}$ were prepared in the following manner. The ferrous deoxy protein was formed by purging the ferric derivative with Ar for 1 h at room temperature, followed by injection of an appropriate amount of sodium dithionite solution (prepared under an Ar atmosphere) to achieve an excess of 100 μM over the heme concentration. Complete reduction of the enzyme was confirmed by optical absorption measurements. Oxygen-containing buffer solutions were prepared by equilibrating deoxygenated buffer with 1 atm of $^{16}O_2$ or $^{18}O_2$. All protein samples and buffers were needle transferred into Hamilton gastight syringes in a glovebox (Vacuum Atmospheres Corp., Hawthorne, CA) with oxygen tensions of <5 parts per million. The oxy intermediates were produced by mixing the deoxy protein samples with oxygen-containing buffers in a homemade submillisecond continuous-flow rapid mixer as described previously.[34] Prior to mixing, oxygen was removed from the system, including the mixer, observation cell, and connecting tubing, by thoroughly purging with a deoxygenated buffer solution. Deoxy $iNOS_{oxy}$ and oxygen-containing buffer were mixed in a one-to-one ratio to achieve a final flow rate of 0.042 mL/s in the observation cell. The oxy complexes were probed at 2 ms following the initiation of the reactions.

Kinetic resonance Raman spectra were obtained by using the 413.1 nm output from a krypton ion laser (Spectra-Physics, Mountain View, CA) to irradiate the samples at room temperature (~25 °C). The laser beam, passing through a band-pass filter, was focused to a ~30 μm spot and directed onto the continuously flowing sample in the quartz observation cell. The incident laser power on the sample was ~40 mW. The scattered light was collected and focused onto an entrance slit (100 μm) of a 1.25 m SPEX spectrophotometer (Jobin Yvon, Edison, NJ) and was then detected using a liquid nitrogen cooled CCD camera (Roper Scientific, Princeton, NJ). Cosmic ray artifacts were removed from the spectra by using a routine in the Winspec spectral acquisition software (Roper Scientific, Princeton, NJ). Data were averaged and accumulated for a total integration time of 3 min per spectrum. Some of the data sets were smoothed with a Fourier smoothing function in the Grams data analysis package (Galactic Industries, Inc.) as indicated.

Equilibrium resonance Raman spectra of the CO adducts were obtained at room temperature (~25 °C) with the 441.6 nm output from a He−Cd laser (Liconix, Santa Clara, CA). The incident laser power on the sample was kept under 3 mW, and the sample cell was rotated at ~6000 rpm during the spectral acquisition to avoid photodamage. Absorption spectra were measured before and after the Raman data acquisition to confirm that there was no sample deterioration due to the laser exposure. Data were averaged and accumulated for a total integration time of 30 min per spectrum. All of the Raman spectra were calibrated with Raman lines from indene, giving an accuracy of ±1 cm^{-1}.

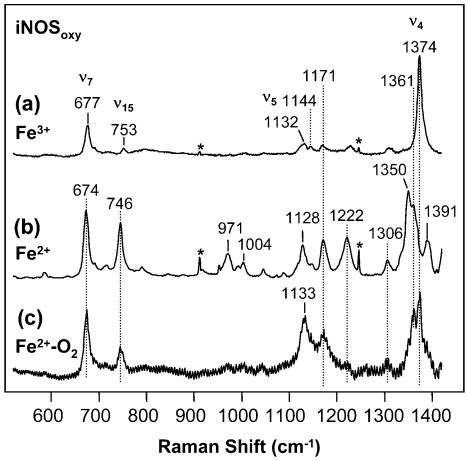

Figure 2. Resonance Raman spectra of substrate- and cofactor-free $iNOS_{oxy}$ in (a) the ferric form, (b) the ferrous form, and (c) the ferrous O_2 complex. The excitation wavelength for the resonance Raman spectra was 413.1 nm. The lines marked with an asterisk (∗) denote the plasma lines from the laser.

Results

Resonance Raman Spectrum of the $Fe^{2+}-O_2$ Complex. Figure 2 shows the resonance Raman spectra of the O_2 complex of the substrate and cofactor-free $iNOS_{oxy}$, as compared to its ferric (Fe^{3+}) and the ferrous deoxy (Fe^{2+}) derivatives. The ν_4 heme vibrational mode in the 1340−1380 cm^{-1} region is very sensitive to the electron density on the heme macrocycle and hence is a good indicator of the oxidation state of the heme iron. In the ferric state, ν_4 was centered at 1374 cm^{-1}, typical for a ferric heme. Upon reduction, a doublet in ν_4, with lines centered at 1350 and 1361 cm^{-1}, was observed. This is consistent with the previously reported spectra of the ferrous complex of $nNOS_{oxy}$, with one component of ν_4 centered at 1347 cm^{-1}, corresponding to a 5C high-spin ferrous state of the enzyme, and a component at 1360 cm^{-1}, resulting from a 6C state.[14] The coexistence of the two states presumably reflects the structural flexibility of the heme active sites of the two NOS isoforms.[14] The other strong lines at 1132, 753, and 677 cm^{-1} in the spectrum of the ferric state, and the corresponding lines at 1128, 746, and 674 cm^{-1} in the ferrous oxidation state, are assigned to ν_5, ν_{15}, and ν_7, respectively.

To examine the short-lived O_2 complex, a homemade continuous-flow mixer with a 100 μs dead time was used. Two spectral lines centered at 1361 and 1373 cm^{-1} associated with the ν_4 modes were observed at 2 ms following the initiation of the binding reaction of O_2 to $iNOS_{oxy}$. We attribute these lines to two different species, the 1373 cm^{-1} line originating from the oxy complex and the 1361 cm^{-1} line from the unreacted deoxy enzyme. These spectral features are similar to those of the oxy complex of $nNOS_{oxy}$.[31] In comparison to the ferric and ferrous states, the oxygen-bound enzyme has a unique and strong vibrational mode centered at 1133 cm^{-1}. When the reaction was carried out with $^{18}O_2$ rather than $^{16}O_2$ (Figure 3, spectra a and b), the intensity of the mode at 1133 cm^{-1} was significantly reduced and a new mode at 1067 cm^{-1} was observed. In the $^{16}O_2-^{18}O_2$ difference spectrum (Figure 3, spectrum c), all the non-O_2-associated porphyrin modes cancel out, and the remain-

(33) Stuehr, D. J.; Ikeda-Saito, M. *J. Biol. Chem.* **1992**, *267*, 20547−20550.
(34) Takahashi, S.; Yeh, S. R.; Das, T. K.; Chan, C. K.; Gottfried, D. S.; Rousseau, D. L. *Nat. Struct. Biol.* **1997**, *4*, 44−50.

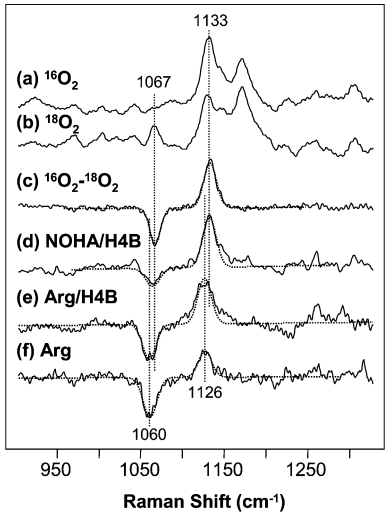

Figure 3. Resonance Raman spectra of the O_2 complexes of $iNOS_{oxy}$. Spectra a−c were obtained from the $^{16}O_2$- and $^{18}O_2$-bound enzyme in the absence of H4B and Arg and the isotope difference spectrum ($^{16}O_2 - {}^{18}O_2$) of the two, respectively, as indicated. Spectra d−f are the isotope difference spectra ($^{16}O_2 - {}^{18}O_2$) obtained in the presence of NOHA/H4B, Arg/H4B, and Arg alone, respectively. Arg, H4B, and NOHA were added in 100×, 3−5×, and 10× excess over the heme content, respectively. The dotted lines are Gaussian fits of the positive and negative components of the isotope difference spectra. The excitation wavelength for the resonance Raman spectra was 413.1 nm.

ing positive and negative peaks are assigned to the O−O stretching modes (ν_{O-O}) associated with the $^{16}O_2$ and $^{18}O_2$ adducts, respectively. Unfortunately, the Fe−O_2 stretching mode is too weak to be detected in the spectra.

To quantify the ν_{O-O} mode, both the negative and positive lines in the isotopic difference spectrum were fitted with single Gaussian curves (dotted lines in Figure 3, spectrum c). The frequencies of the two peaks were identified at 1133 and 1067 cm^{-1} with widths of 18 and 16 cm^{-1}, respectively. These frequencies indicate that the O_2 complex of $iNOS_{oxy}$ exists predominantly as the ferric−superoxide configuration (species IV in Figure 1) rather than a ferrous−dioxygen complex (species III), consistent with the dioxygen complexes of other heme proteins.[31] The observed isotope frequency shift, $\Delta\nu_{O-O} = 66$ cm^{-1}, is in agreement with the theoretical value (65 cm^{-1}) predicted by treating the O_2 as a diatomic harmonic oscillator. The residual intensity of the 1133 cm^{-1} peak observed in the $^{18}O_2$ complex (Figure 3, spectrum b) indicates that the ν_{O-O} mode of the $^{16}O_2$ complex overlaps with a porphyrin vibrational mode centered at 1133 cm^{-1}, as was also seen in $nNOS_{oxy}$ and in other heme proteins.[35,36] Fortunately, it does not appear to couple to the ν_{O-O} mode, since the spectral shapes and intensities of the two isotope lines are similar and the isotope shift is close to the theoretical value.

Substrate−Ligand Interaction in the Fe^{2+}−O_2 Complex. To study the influence of substrates on the structural properties of the oxy complex of $iNOS_{oxy}$, the oxygen reaction was carried out with either the Arg- or NOHA-bound protein, in the presence and absence of H4B. Figure 3 shows the isotopic difference spectra between the $^{16}O_2$- and $^{18}O_2$-bound proteins under various conditions. In the presence of Arg alone (spectrum f), the ν_{O-O} mode shifted to 1126 cm^{-1}, but the peak width remained almost constant as compared to that of the substrate-free protein (16 vs 18 cm^{-1}). The 7 cm^{-1} shift suggests a direct interaction between Arg and the heme-bound dioxygen. A similar frequency shift was detected in the Arg and H4B-bound protein (spectrum e), demonstrating that the binding of H4B does not induce significant structural changes to the complex. In contrast to the effect of Arg, the ν_{O-O} mode of the NOHA and H4B-bound protein (spectrum d) was found at 1132 cm^{-1} with a width of 16 cm^{-1}, the same as that of the substrate-free $iNOS_{oxy}$. No other oxygen-sensitive lines were detected in the 500−1400 cm^{-1} spectral range for all of the conditions studied.

Table 1 summarizes the positions of the ν_{O-O} modes of $iNOS_{oxy}$ under various conditions as compared to those obtained from other heme proteins, including $nNOS_{oxy}$, a bacterial NOS from *Staphylococcus aureus* (saNOS, *Staphylococcus aureus* nitric oxide synthase), cytochrome P450s and its model systems, and hemoglobin derivatives. To further investigate if the shifts in the ν_{O-O} mode in $iNOS_{oxy}$ originate from a direct interaction with the substrate or an indirect effect due to structural changes induced by substrate binding, the resonance Raman spectra of the CO-bound derivatives were examined in the absence and presence of the substrates.

Substrate−Ligand Interaction in the Fe^{2+}−CO Complex. The low-frequency resonance Raman spectra of the Fe^{+2}−CO complex of the substrate-free, NOHA-bound, and Arg-bound $iNOS_{oxy}$ are shown in Figure 4. In the substrate-free protein, the Fe−CO stretching mode is broad and centered at ∼491 cm^{-1}. It can be deconvoluted into two Gaussian peaks centered at 482 and 502 cm^{-1} with equal widths of 26 cm^{-1} as shown in the right panel in Figure 4. The data suggest the presence of two distinct conformations. Binding of NOHA to the protein shifts the equilibrium toward the 502 cm^{-1} form; in addition, a weak shoulder at 512 cm^{-1} with similar bandwidth (28 cm^{-1}) was detected. When Arg is bound, the broad ν_{Fe-CO} mode shifts to a sharp peak centered at 512 cm^{-1} as previously reported,[37] in addition to residual contributions from the 482 and 502 cm^{-1} peaks. The presence of these multiple Fe−CO lines is confirmed in the CO isotope difference spectra (data not shown).[30,37,38]

The ν_{C-O} mode of the Arg-bound $iNOS_{oxy}$ was found at 1907 cm^{-1} (see the Supporting Information, Figure S1, spectrum b); on the other hand, that of the NOHA-bound derivative (spectrum c) has features centered at ∼1904 and ∼1930 cm^{-1}, although the exact positions of the latter two bands could not be accurately determined due to the poor signal-to-noise ratio of the spectrum. Combined with the ν_{Fe-CO} data shown in Figure 4, we assign the two modes to two conformers, one with ν_{Fe-CO} and ν_{C-O} modes at 512 and 1904 cm^{-1}, respectively, and the other with the modes at 502 and 1930 cm^{-1}, respectively, since ν_{Fe-CO} and ν_{CO} are inversely correlated (vide infra). In the absence of substrate, two ν_{Fe-CO} modes at 482 and 502 cm^{-1} were observed (Figure 4); however, only a broad feature roughly centered at ∼1945 cm^{-1} was identified for the ν_{C-O} mode (Supporting Information, spectrum a in Figure S1), which is too broad to be deconvoluted reliably. Nonetheless, the ν_{C-O} mode may be roughly accounted by a combination of two peaks at ∼1962 and 1930 cm^{-1}, associated with the 482 and 502 cm^{-1}

(35) Kerr, E. A.; Yu, N. T.; Bartnicki, D. E.; Mizukami, H. *J. Biol. Chem.* **1985**, *260*, 8360−8365.
(36) Hu, S.; Schneider, A. J.; Kincaid, J. R. *J. Am. Chem. Soc.* **1991**, *113*, 4815−4822.
(37) Li, D.; Stuehr, D. J.; Yeh, S. R.; Rousseau, D. L. *J. Biol. Chem.* **2004**, *279*, 26489−26499.
(38) Wang, J.; Stuehr, D. J.; Rousseau, D. L. *Biochemistry* **1997**, *36*, 4595−4606.

Table 1. Comparison of the ν_{O-O} of $iNOS_{oxy}$, $nNOS_{oxy}$, saNOS, Cytochrome P450cam, Model Complexes, and Hemoglobins[a]

protein	ligand	binding state	ν_{O-O}, cm^{-1}	ν_{Fe-CO}, cm^{-1} [b] ν_{max}	width	intensity (%)	ref
$iNOS_{oxy}$	Cys^-	none	1133 (1067)	482	26	67	this work
				502	26	33	
		NOHA + H4B	1132 (1066)	481	26	31	this work
				500	26	53	
				513	28	16	
		Arg ± H4B	1126 (1060)	482	26	11	this work
				503	26	34	
				512	15	55	
$nNOS_{oxy}$	Cys^-	none	1132 (1068)	489	26	80	31, this work
				501	12	14	
				514	12	6	
		NOHA ± H4B	1132 (1068)	490	26	56	31, this work
				501	12	30	
				514	12	14	
		Arg ± H4B	1130 (1068)	489	26	52	31, this work
			1122 (1056)	502	12	28	
				514	12	20	
saNOS	Cys^-	none	1135 (1071)	482			44
				497			44
		Arg ± H4B	1135 (1071)	504			
			1123 (1062)				
$P450_{cam}$	Cys^-	none	1147				36, 35
		adamantanone	1139 (1074)	474			36, 65
			1147 (1080)				
		camphor	1139 (1073)	481			36, 65
TpivPP	$C_6HF_4S^-$	1140					36, 66
	$C_6F_5S^-$	1147					36
Co−Hb	His	1139					67
Fe−Hb	His	1132					68

[a] Frequencies obtained with $^{18}O_2$ are indicated in parentheses. The ν_{Fe-CO} for the various proteins are listed as comparisons. [b] The iNOS and nNOS data were obtained on the basis of the peak deconvolution shown in Figure 4 and Supporting Information Figure S2.

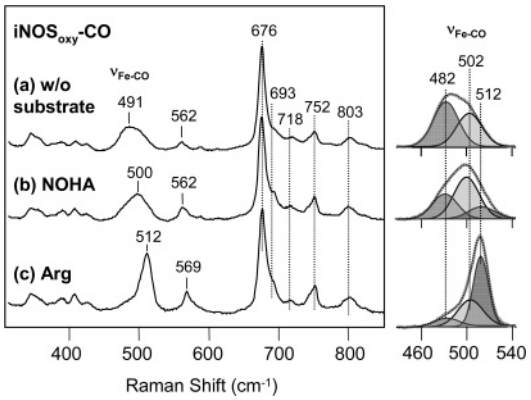

Figure 4. Resonance Raman spectra of the CO complex of $iNOS_{oxy}$ in the absence of H4B and Arg (a) and in the presence of NOHA (b) and Arg (c). The right panel shows the spectral deconvolution results of the corresponding ν_{Fe-CO} modes. The peak positions and the bandwidths of the Gaussian peaks that comprise each ν_{Fe-CO} mode are listed in Table 1. The excitation wavelength for the resonance Raman spectra was 441.6 nm.

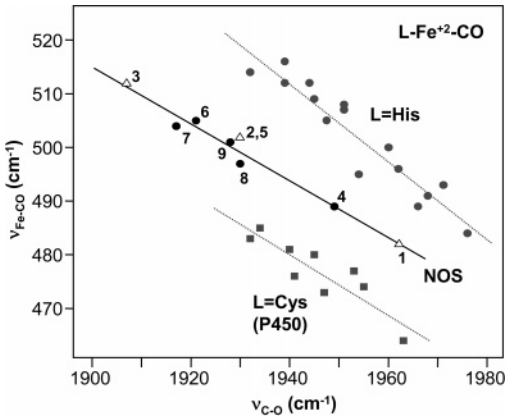

Figure 5. Inverse correlation curve between ν_{CO} and ν_{Fe-CO} in the CO derivatives of heme proteins coordinated with a histidine proximal ligand or thiolate proximal ligand, including the NOS and P450 enzyme families. Data points 1−3, 4 and 5, 6 and 7, and 8 and 9 are the conformers from $iNOS_{oxy}$, $nNOS_{oxy}$, saNOS (ref 63), and gsNOS (*Geobacillus stearothermophilus* NOS) (Kabir, M. et al., to be published), respectively. All other points were taken from prior reports of the inverse correlation (refs 39 and 64).

conformers, respectively, as predicted by the ν_{Fe-CO} and ν_{CO} inverse correlation curve discussed below.

The ν_{Fe-CO} and ν_{CO} modes of CO-bound heme proteins are typically inversely correlated (Figure 5), as a result of the back-bonding from the d_π orbital of the heme iron to the empty π^* orbital of the CO.[39] The changes in the polarity of the distal heme environment affect the degree of the back-bonding, thereby shifting the data points along the correlation curve. This effect was elegantly demonstrated in sperm whale myoglobin mutants by Phillips et al., who showed that the electrostatic potential of the protein environment surrounding the heme-bound CO correlates quantitatively with ν_{Fe-CO} and inversely with ν_{C-O}.[40] On the other hand, changes in the bonding properties of the proximal iron−ligand bond affect the offset of the correlation curve, due to the competition between the proximal and distal ligands for σ-bonding to the d_{z^2} orbital of the heme iron. Consequently, the correlation line for thiolate-ligated heme proteins (e.g., P450s) is distinct from that for the

(39) Yu, N.-T.; Kerr, E. A. In *Biological Applications of Raman Spectroscopy*; Spiro, T. G., Ed.; John Wiley & Sons: New York, 1987; Vol. 3, pp 39−96.

(40) Phillips, G. N.; Teodoro, M. L.; Li, T.; Smith, B.; Olson, J. S. *J. Phys. Chem. B* **1999**, *103*, 8817−8829.

histidine-ligated heme proteins (e.g., hemoglobins) and that for the 5C CO-bound model compounds. Intriguingly, although NOS, like the P450 groups of enzymes, has a Cys residue as the proximal ligand, the correlation line for the various NOS derivatives, including mammalian and bacterial NOSs, is located higher than that of the P450s and lower than that of the histidine-ligated heme proteins.[30,41] The offset of the NOS line from the P450 line has been attributed to the weaker electron-donating capability of the proximal Cys in NOS as compared to that of P450, as reflected by the 13 cm^{-1} lower Fe−Cys stretching frequency of NOS.[30,41]

The data point (no. 3) of the major conformer of the Arg-bound $iNOS_{oxy}$, associated with ν_{Fe-CO} and ν_{C-O} at 512 and 1907 cm^{-1}, respectively, sits at the upper left corner of the NOS correlation line (Figure 5), reflecting a strong positive electrostatic potential surrounding the heme-bound CO, presumably due to direct H-bonding interactions between the ligand and the substrate. The data points of the minor conformers of the Arg adduct, associated with ν_{Fe-CO} at 482 and 502 cm^{-1}, could not be directly identified because the ν_{C-O} modes were not detected due to their weak intensities. Nonetheless, the data associated with the 502 cm^{-1} conformer is also present in the NOHA-bound protein as the major component, which is associated with ν_{C-O} at 1930 cm^{-1}. The data point (no. 2) lies in the middle of the correlation line, indicating a reduced electrostatic potential in comparison to the conformer no. 3. The conformer associated with ν_{Fe-CO} at 482 cm^{-1} is dominant in the absence of substrate; although the ν_{C-O} mode is too weak and too broad to be clearly identified in the spectra, the data point (no. 1) may be estimated by extrapolation of the inverse correlation line. The datum is located at the lower right corner, indicating low electrostatic potential in comparison to the other two conformers. The datum of the minor conformer of the NOHA-bound protein, with ν_{Fe-CO} and ν_{C-O} at 512 and 1904 cm^{-1}, respectively, lies on the same location as the data point no. 3.

If the frequency differences in the ν_{Fe-CO} and ν_{C-O} were a result of long-range conformational changes that modified the proximal iron−Cys bond or the geometries of the heme peripheral groups, deviations from the correlation curve would be expected. The observation that the data points associated with the various derivatives of $iNOS_{oxy}$ all lay on the same ν_{Fe-CO} versus ν_{C-O} correlation curve is hence consistent with a scenario in which the spectral differences are due to direct distal interactions with the ligand. Taken together the data show that the substrate-free $iNOS_{oxy}$ exhibits two conformations: the 482 cm^{-1} form with negative or neutral electrostatic potential and the 502 cm^{-1} form with a more positive electrostatic potential. Binding NOHA to the protein increases the population of the 502 cm^{-1} and introduces a new conformation, associated with ν_{Fe-CO} at 512 cm^{-1} that displays high positive electrostatic potential. Binding of Arg locks the protein in the 512 cm^{-1} form with a reduced conformational freedom as indicated by the reduction of the bandwidth from 26 to 15 cm^{-1} (Table 1). The intrinsically weaker interaction between NOHA and the Fe^{+2}−CO moiety in $iNOS_{oxy}$ is consistent with the insensitivity of ν_{O-O} in the oxy complex to NOHA binding (Figure 3).

Intriguingly, the effect of substrate binding on the Fe−CO moiety in the CO-bound $nNOS_{oxy}$ is distinct from $iNOS_{oxy}$. The ν_{Fe-CO} of the substrate-free protein is dominated by two peaks centered at 489 and 501 cm^{-1}, as well as a very small component at 514 cm^{-1} (see Figure S2 in the Supporting Information). The intensities of the 501 and 514 cm^{-1} components are enhanced upon either NOHA or Arg binding, without any significant differences between the two substrate-bound states. Unlike that found in $iNOS_{oxy}$, the bandwidth of the 501 cm^{-1} component (∼12 cm^{-1}) is as narrow as the 514 cm^{-1} peak. The reduced sensitivity of the ν_{Fe-CO} to Arg binding in $nNOS_{oxy}$ with respect to $iNOS_{oxy}$ (see Table 1) is consistent with the observation that the ν_{O-O} mode of the O_2 complex of $nNOS_{oxy}$ is less sensitive to Arg binding than that in $iNOS_{oxy}$.[30]

Discussion

The frequency of the O−O stretching mode in heme proteins and model complexes has been shown to be modulated by several factors, including direct interactions between the bound ligand and the residues or substrates situated in the distal pocket, cis effects due to variations in the heme macrocycle or its peripheral constituents, and trans effects due to changes in the electronic properties of the proximal ligand.[39] In the case of the O_2 complex of NOS, we attribute the frequency changes to distal electrostatic effects as demonstrated in Figure 5. Recently, Lu et al. have systematically determined the electrostatic effects on the structural properties of the Fe−O−O moiety in a truncated hemoglobin from *C. jejuni*, by mutating the key distal polar residues, which form H-bonds with the heme-bound dioxygen in the wild-type protein, to nonpolar substituents.[42] It was found that the frequency of the ν_{O-O} mode is sensitive to the regioorientation of the H-bonds and it can be lowered by up to 12 cm^{-1} upon the mutation, consistent with the observation reported here for $iNOS_{oxy}$ as discussed below.

Isoform-Specific Substrate−O_2 Interactions. The ν_{O-O} of the O_2 complexes of several thiolate-coordinated heme proteins have been reported as listed in Table 1.[36,43] In P450cam, the ν_{O-O} mode was found at 1147 cm^{-1}, the addition of camphor caused it to shift to 1139 cm^{-1}, whereas the binding of adamantanone led to equal components at 1147 and 1139 cm^{-1}.[36,43] The ν_{O-O} mode of the O_2-bound $nNOS_{oxy}$ was previously found at 1132 cm^{-1} and was reported to be insensitive to the presence of added substrates and cofactor;[31] however, later refined analysis revealed that Arg binding caused a small shift of the peak by ∼2 cm^{-1}; in addition, it is associated with the development of a small shoulder at ∼1122 cm^{-1} with ∼10% of the intensity of the parent peak.[30] Likewise, in saNOS, the ν_{O-O} of the substrate-free form was detected at 1135 cm^{-1}. Arg binding to the saNOS led to the presence of the 1123 cm^{-1} peak, in addition to the parental 1135 cm^{-1} peak (here these two peaks exhibited almost equal intensity).[44] Similar to that of $nNOS_{oxy}$ and saNOS, the ν_{O-O} mode of the substrate-free $iNOS_{oxy}$ was identified at 1133 cm^{-1}; however, Arg binding caused the shift of the entire peak to 1126 cm^{-1} (Figure 3), indicating a stronger substrate−ligand interaction in $iNOS_{oxy}$ with respect to $nNOS_{oxy}$ and saNOS.

(41) Schelvis, J. P.; Berka, V.; Babcock, G. T.; Tsai, A. L. *Biochemistry* **2002**, *41*, 5695−5701.
(42) Lu, C.; Egawa, T.; Wainwright, L. M.; Poole, R. K.; Yeh, S. R. *J. Biol. Chem.* **2007**, *282*, 13627−13636.
(43) Sjodin, T.; Christian, J. F.; Macdonald, I. D.; Davydov, R.; Unno, M.; Sligar, S. G.; Hoffman, B. M.; Champion, P. M. *Biochemistry* **2001**, *40*, 6852−6859.
(44) Chartier, F. J.; Blais, S. P.; Couture, M. *J. Biol. Chem.* **2006**, *281*, 9953−9962.

The changes in the ν_{O-O} mode in response to substrate binding in the NOS and P450 proteins are a result of the perturbation in the electrostatic potential of the active heme ligand-binding site introduced by the presence of the substrate. These same types of interactions are seen in the CO derivatives despite the fact that the binding geometry is linear with CO rather than being bent as in the O_2 case (Table 1). In the CO derivatives of P450cam, the camphor-bound protein exhibits ν_{Fe-CO} at 481 cm^{-1}, whereas that in the adamantanone-bound protein is at 474 cm^{-1}, indicating the higher electrostatic potential due to the presence of camphor, as compared to adamantanone, in the distal pocket. The higher electrostatic potential associated with the camphor-bound protein presumably forces the oxy derivative to be locked in a single conformation associated with a single ν_{O-O} at 1139 cm^{-1}, with respect to the two conformations associated with ν_{O-O} at 1139 and 1147 cm^{-1} in the adamantanone-bound protein.

In the CO derivatives of $iNOS_{oxy}$, three conformers associated with ν_{Fe-CO} at 489, 502, and 512 cm^{-1} (Figure 4) were observed. In the substrate-free form of $iNOS_{oxy}$, the ν_{Fe-CO} is dominated by the two low-frequency components at 489 and 502 cm^{-1}. The 512 cm^{-1} mode is preferentially observed in the presence of Arg, and it is significantly narrower (bandwidth ~12 cm^{-1}, see Table 1) as compared to that of the 489 cm^{-1} mode (26 cm^{-1}), suggesting its reduced conformational freedom due to direct H-bonding interactions between the ligand and substrate. NOHA binding leads to an increase in the intensity of the high-frequency modes at 502 and 512 cm^{-1}, indicating the redistribution of the population of the conformational states, favoring those associated with higher electrostatic potential. Interestingly, the electrostatic potential exerted by NOHA is not as strong as that imposed by Arg as indicated by the fact that the ν_{Fe-CO} is dominated by the 502 cm^{-1} component, instead of the 512 cm^{-1} mode (Figure 4). The data clearly demonstrated that, like the oxy complex, stronger ligand−substrate interactions are present in the Arg adduct with respect to the NOHA adduct. In contrast to $iNOS_{oxy}$, in $nNOS_{oxy}$, the high-frequency component at 514 cm^{-1} in the CO adduct is only slightly enhanced in the Arg-bound protein with respect to the NOHA-bound derivative. This is consistent with the small differences in the ν_{O-O} mode between the two substrate-bound adducts of $nNOS_{oxy}$.[30]

The presence of the two ν_{O-O} modes in the oxy derivatives of Arg-bound $nNOS_{oxy}$ agrees well with the multiple binding conformations of Arg in nNOS reported by Gorren et al.[45] The multiple binding conformations of Arg were found to be isoform-specific, which is consistent with the differential response of the ν_{O-O} mode to Arg binding in $nNOS_{oxy}$ versus $iNOS_{oxy}$. Along the same lines, ENDOR studies show that the position of the substrate in nNOS is distinct from that in iNOS.[46] Furthermore, crystallographic data showed that the hydrogen-bonding interactions between CO and Arg are weaker in $nNOS_{oxy}$ with respect to $eNOS_{oxy}$; the latter is structurally analogous to the $iNOS_{oxy}$ as suggested by their similar Raman spectroscopic properties.[47,48] Collectively, these data support our conclusion that the structural properties of oxy complexes of $iNOS_{oxy}$ and $nNOS_{oxy}$ are distinct.

Structural Implications. The crystal structures of all three mammalian NOS isoforms and two bacterial NOS (saNOS and asNOS) are available in various ligand and substrate-bound states.[10−13,49−52] In $iNOS_{oxy}$, the Arg lies over the heme with its terminal nitrogen atom located ~3.8 Å from the iron atom. The guanidinium group of the Arg forms H-bonds with the side-chain group of the Glu371 residue and the backbone carbonyl group of the Trp366 residue, as well as a water molecule that is ~2.7 Å away (see Figure S3b in the Supporting Information).[10] A similar structure was reported for $nNOS_{oxy}$ as shown in Supporting Information Figure S3d.[50] When CO or NO is bound in $nNOS_{oxy}$, in addition to the above-mentioned H-bonding network, the oxygen atom of the ligand accepts H-bonds from the water molecule and the guanidinium group of the Arg.[50,52] Equivalent ligand−substrate interactions were also reported in $eNOS_{oxy}$[49] and *Bacillus subtilis* NOS (bsNOS, *Bacillus subtilis* nitric oxide synthase).[51,52]

In the substrate-free form of $iNOS_{oxy}$, three water molecules have been reported in the distal pocket as shown in Supporting Information Figure S3a. The first water occupies a similar position as that found in the Arg-bound protein. The second water, like the Arg in the Arg-bound protein, forms H-bonds with the side-chain group of the Glu371 residue and the backbone carbonyl group of the Trp366 residue. The last water molecule forms an addition H-bond with the side-chain group of the Glu371. Although we recognize that the identification of solvent molecules in crystal structures can be tenuous, the presence of these water molecules could account for the positive polar distal environment of the substrate-free $iNOS_{oxy}$ as revealed by the resonance Raman data of the CO derivative (Figure 4). In the NOHA-bound $iNOS_{oxy}$, the terminal hydroxy group of the substrate, NOHA, is engaged in an H-bond interaction with the peptide nitrogen from the nearby Gly365 residue.[53] This additional interaction may account for the fact that iNOS possesses higher affinity for NOHA than L-Arg.[18] Furthermore, the additional H-bond may pull the substrate slightly away from the heme ligand, thereby accounting for the reduced electrostatic potential of the active site, with respect to the Arg-bound protein, as suggested by the data shown in Figure 4. Taken together these data suggest that the differential response of ν_{O-O} to Arg with respect to NOHA binding in the oxy derivative of $iNOS_{oxy}$ and $nNOS_{oxy}$ result from the differing H-bonding network surrounding the heme-bound dioxygen.

Up to now, there is no crystal structure available for the O_2-bound derivative of any of the NOS proteins. In the O_2-bound P450cam, a water molecule and a nearby Thr residue were found to donate H-bonds to the terminal oxygen atom of the heme-bound dioxygen;[54] based on the well-known push−pull model, the H-bonds provide an electronic pull for the activation of the O−O bond. It also offers an essential proton for the protonation of the terminal oxygen for its conversion to a water molecule

(45) Gorren, A. C.; Schmidt, K.; Mayer, B. *Biochemistry* **2002**, *41*, 7819−7829.
(46) Tierney, D. L.; Huang, H.; Martasek, P.; Roman, L. J.; Silverman, R. B.; Masters, B. S.; Hoffman, B. M. *J. Am. Chem. Soc.* **2000**, *122*, 5405−5406.
(47) Li, D.; Hayden, E. Y.; Panda, K.; Stuehr, D. J.; Deng, H.; Rousseau, D. L.; Yeh, S. R. *J. Biol. Chem.* **2006**, *281*, 8197−8204.
(48) Fan, B.; Wang, J.; Stuehr, D. J.; Rousseau, D. L. *Biochemistry* **1997**, *36*, 12660−12665.
(49) Li, H.; Raman, C. S.; Martasek, P.; Masters, B. S.; Poulos, T. L. *Biochemistry* **2001**, *40*, 5399−5406.
(50) Li, H.; Igarashi, J.; Jamal, J.; Yang, W.; Poulos, T. L. *J. Biol. Inorg. Chem.* **2006**, *11*, 753−768.
(51) Pant, K.; Bilwes, A. M.; Adak, S.; Stuehr, D. J.; Crane, B. R. *Biochemistry* **2002**, *41*, 11071−11079.
(52) Pant, K.; Crane, B. R. *Biochemistry* **2006**, *45*, 2537−2544.
(53) Crane, B. R.; Arvai, A. S.; Ghosh, S.; Getzoff, E. D.; Stuehr, D. J.; Tainer, J. A. *Biochemistry* **2000**, *39*, 4608−4621.
(54) Nagano, S.; Poulos, T. L. *J. Biol. Chem.* **2005**, *280*, 31659−31663.

following the rupture of the O−O bond.[55,56] Our resonance Raman data support the scenario that the reaction of Arg to NOHA in NOS follows the P450-like reaction mechanism, as that suggested by others.[20,21] We propose that the water molecule reported in the crystal structure of the Arg-bound $iNOS_{oxy}$ plays a similar role as that found in P450cam. In addition, the longer distance between the water molecule and the guanidinium N^{ω} group of Arg in $nNOS_{oxy}$ as compared to $iNOS_{oxy}$ may account for the lower sensitivity of ν_{O-O} to Arg-binding in the former as compared to the latter.

The distinct ν_{O-O} of the NOHA-bound oxy complex of $iNOS_{oxy}$ with respect to that of the Arg-bound complex suggests that the second step of the NOS reaction follows a different reaction path, as has been proposed by Pant and Crane based on crystallographic studies of bsNOS.[52] In the NO derivative of ferrous bsNOS, the N^{ω} atom of NOHA is only 2.6 Å away from the nitrogen atom of the heme-bound NO, suggesting a possible H-bonding interaction between the $N^{\omega}H$ of the NOHA and the proximal oxygen atom of the heme-bound dioxygen in the oxy derivative.[52] The H-bond to the proximal oxygen atom, which is coordinated to the heme iron, would be expected to have less of an effect on the O−O stretching mode than the H-bond to the terminal oxygen atom. We hypothesize that the NOHA to citrulline conversion follows a heme oxygenase (HO)-like mechanism. In HO, unlike P450s, the active intermediate that carries out the electrophilic attack on the α-meso carbon of the heme is the heme-bound peroxide, instead of a ferryl species; in addition, to prevent the premature bond-cleavage reaction, the proximal O atom of the heme-bound dioxygen is H-bonded with a nearby amino acid residue.[57−59] We propose that, like HO, in the second step of the NOS reaction, the proximal oxygen atom of the dioxygen accepts a H-bond from the $N^{\omega}H$ group of NOHA and it is the terminal oxygen atom that is incorporated into the substrate via a nucleophilic addition reaction. Consistent with this proposal, in the NO adduct of ferrous bsNOS, the oxygen atom of the iron-bound NO (analogous to the terminal oxygen of the dioxygen in the peroxy intermediate) is only 3.6 Å away from the guanidinium carbon atom, close enough for the execution of the nucleophilic attack.[52]

Mechanistic Implications. On the basis of the substrate−O_2 interactions revealed by the resonance Raman studies, we postulate the following mechanism for the two steps of the NOS catalytic reaction as illustrated in Figure 6. In the first step of the reaction, the enzyme, reduced by electron transfer from the reductase domain, binds an O_2 molecule to form the ferric superoxide complex (I). The terminal oxygen atom of the iron-bound dioxygen accepts H-bonds from the guanidinium group of the Arg and the water molecule H-bonded to it. A peroxy intermediate (II) is subsequently formed following an electron transfer from H4B to the iron-bound dioxygen, leaving a radical on the H4B as demonstrated by the EPR measurements.[19] The subsequent O−O bond-cleavage reaction, facilitated by the two H-bonds at the peroxide terminal oxygen atom, leads to a ferryl species (III). The ferryl oxygen atom undergoes an electrophilic attack on the amine nitrogen of the Arg, generating intermediate IV, which spontaneously rearranges to the ferric heme and NOHA (V).[60] The first half of the NOS reaction cycle is completed by the transfer of a second electron from the reductase domain to the H4B radical bringing it back to its neutral form. In this scheme, the Arg and NOHA are presented in their protonated forms, in which the N^{ω} atom of the guanidium group is protonated, as suggested by previous studies.[61]

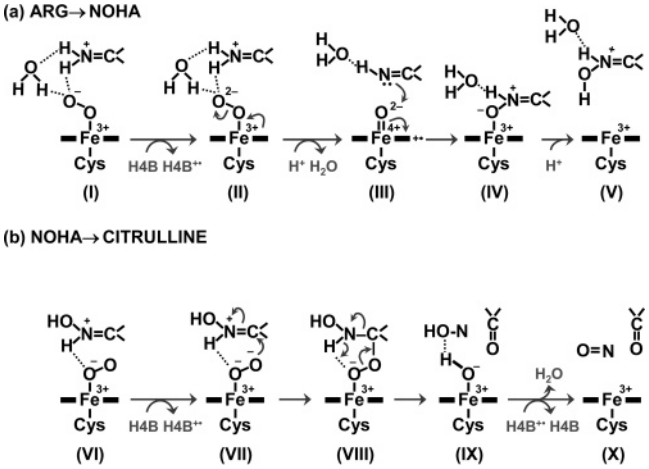

Figure 6. Proposed mechanisms for the first and second steps of the NOS reaction as discussed in the text.

In the second step of the reaction, the ferric heme product from the first step is reduced by an electron transfer from the reductase domain, and another oxygen molecule binds to the heme iron generating a ferric superoxide complex (VI), as observed in the first step of the reaction. Unlike the first step of the reaction though, in the superoxide complex it is the proximal oxygen, not the terminal oxygen, which accepts an H-bond form the N^{ω} proton of the substrate NOHA. When an electron is transferred from the H4B to the dioxygen, a peroxy intermediate (VII) is generated, just as in the first step, leading to a radical species, which was detected by EPR measurements on the same time scale as the disappearance of the superoxide species.[22] However, due to the absence of the H-bonds to the terminal oxygen atom, the O−O bond of the peroxy intermediate is not cleaved as in the first step of the NOS reaction; instead, the peroxy moiety undergoes a nucleophilic attack on the guanidinium carbon atom, forming a tetrahedral intermediate (VIII). The tetrahedral intermediate, in a five-membered ring structure, spontaneously rearranges to citrulline and a protonated nitroxyl anion (HNO) (IX). The latter coverts to a NO radical by giving up its electron, and possibly a proton as well, to the H4B radical, thereby regenerating the neutral H4B cofactor (X).

Conclusions

The data reported here offer clear evidence for the two distinct mechanisms associated with the two steps of the NOS reaction, determined by the nature of the enzymatic substrate. We show that it is the intricate distal H-bonding network between the substrate, water, and the iron bond dioxygen that modulates the fate of the key peroxy intermediate. With the Arg substrate in the first step of the reaction, the O−O bond of the peroxy

(55) Poulos, T. L. *Adv. Inorg. Biochem.* **1988**, *7*, 1−36.
(56) Sono, M.; Roach, M. P.; Coulter, E. D.; Dawson, J. H. *Chem. Rev.* **1996**, *96*, 2841−2888.
(57) Davydov, R.; Matsui, T.; Fujii, H.; Ikeda-Saito, M.; Hoffman, B. M. *J. Am. Chem. Soc.* **2003**, *125*, 16208−16209.
(58) Unno, M.; Matsui, T.; Chu, G. C.; Couture, M.; Yoshida, T.; Rousseau, D. L.; Olson, J. S.; Ikeda-Saito, M. *J. Biol. Chem.* **2004**, *279*, 21055−21061.
(59) Poulos, T. L. *Drug Metab. Dispos.* **2005**, *33*, 10−18.
(60) Meunier, B.; de Visser, S. P.; Shaik, S. *Chem. Rev.* **2004**, *104*, 3947−3980.
(61) Cho, K. B.; Gauld, J. W. *J. Am. Chem. Soc.* **2004**, *126*, 10267−10270.

intermediate is activated to generate the active ferryl species that is capable of oxidizing Arg to NOHA; on the other hand, in the presence of NOHA during the second step of the reaction, the integrity of the O−O bond of the peroxy intermediate produced is conserved prior to its nucleophilic addition to NOHA. To allow for the execution of the two mechanistically distinct reactions in a single enzyme, in addition to the substrate-dependent H-bonding network, apparently the electron-donating strength of the proximal thiolate, coordinated to the heme iron, is elegantly modulated by H-bonding interactions with a nearby Trp residue, which is absent in P450s, as demonstrated by the distinct inverse ν_{Fe-CO} versus ν_{O-O} correlation curves of NOS and P450 shown in Figure 5, as well as those shown in other studies.[62] Unfortunately, confirmation of the intermediates formed during each step of the reaction, other than the primary O_2 complexes, is challenging as they have shorter lifetimes than that of the primary O_2 complexes. Nevertheless, it is anticipated that new approaches and the use of bacterial NOS analogues may help resolve these issues.

Acknowledgment. This work was supported by National Institutes of Health Grants CA53914 and GM51491 (to D.J.S.), HL65465 (to S.-R.Y.), and GM54806 (to D.L.R.). D.L. and M.K. are supported by the Medical Scientist Training Program (GM07288). D.L is also supported by the Molecular Biophysics Training Grant (GM08572) at Albert Einstein College of Medicine.

Supporting Information Available: The difference spectra ($^{12}C^{16}O - {}^{12}C^{18}O$) in the C−O stretching mode region for iNOSoxy in the absence of substrate, in the presence of Arg, and in the presence of NOHA (Figure S1), resonance Raman spectra of the CO complex of $nNOS_{oxy}$ in the absence and presence of substrates and cofactors (Figure S2), and the active site structures for $iNOS_{oxy}$ and $nNOS_{oxy}$ (Figure S3). This material is available free of charge via the Internet at http://pubs.acs.org.

JA070683J

(62) Couture, M.; Adak, S.; Stuehr, D. J.; Rousseau, D. L. *J. Biol. Chem.* **2001**, *276*, 38280−38288.
(63) Chartier, F. J.; Couture, M. *Biophys. J.* **2004**, *87*, 1939−1950.
(64) Spiro, T. G.; Wasbotten, I. H. *J. Inorg. Biochem.* **2005**, *99*, 34−44.
(65) Bangcharoenpaurpong, O.; Rizos, A. K.; Champion, P. M.; Jollie, D.; Sligar, S. G. *J. Biol. Chem.* **1986**, *261*, 8089−8092.
(66) Chottard, G.; Schappacher, M.; Ricard, L.; Weiss, R. *Inorg. Chem.* **1984**, *23*, 4557−4561.
(67) Proniewicz, L. M.; Kincaid, J. R. *J. Am. Chem. Soc.* **1990**, *112*, 675−681.
(68) Alben, J. O.; Bare, G. H.; Moh, P. P. In *Biochemical and Clinical Aspects of Hemoglobin Abnormalities*; Caughy, W. S., Ed.; Academic Press, Inc.: New York, 1978; pp 607−617.